Magnetization reversal mechanisms in Fe/NiO bilayers grown onto nanoporous alumina membranes and Si wafers

Enrique Navarro,[1] María Alonso,[1] Ana Ruiz,[1] Unai Urdiroz,[1] Marta Sánchez-Agudo,[2] Federico Cebollada,[2] (iD)
Guillermo Domíguez-Cañizares,[3] Leonardo Soriano,[3] Alejandro Gutierrez,[3] F. Javier Palomares,[1] (iD)
and Jesús M. González[1,a] (iD)

AFFILIATIONS

[1] Nanostructures and Surfaces, Instituto de Ciencia de Materiales de Madrid, Madrid, 28049 Madrid, Spain
[2] POEMMA-CEMDATIC, Universidad Politécnica de Madrid, Madrid, 28040 Madrid, Spain
[3] Departamento de Física Aplicada, Universidad Autónoma de Madrid, Madrid, 28049 Madrid, Spain

Note: This paper was presented at the 64th Annual Conference on Magnetism and Magnetic Materials.
[a] Corresponding author e-mail jm.g@csic.es

ABSTRACT

We report on the magnetization reversal measured in two ferromagnetic/antiferromagnetic (F/AF) bilayer series: Fe/NiO/Al_2O_3 (nanoporous membranes, series N) and Fe/NiO/Si (wafers, series W). The Fe and NiO layers were deposited by pulsed laser ablation and magnetron sputtering, respectively. In both series different oxygen partial pressures were implemented in the Ar plasma during the NiO growth. The morphologies of both series (as imaged by atomic force microscopy) reflect those of their substrates and, particularly, the series N samples exhibit a six-fold columnar growth around each one of the membranes nanopores. The in-plane hysteresis loops measured upon field cooling the samples down to different temperatures in the range from 50 K up to 290 K evidenced i) 50 K, 0% oxygen coercivities that decreased markedly in both series samples with the increase of the Fe layer thickness (particularly the Fe 5 nm, series N sample exhibited a coercivity larger than the Fe magneto-crystalline anisotropy field), ii) a decrease of the coercivity with the increase of the NiO deposition oxygen partial pressure, observed in both series independently of the Fe layer thickness, iii) low temperature coercivities larger in the series N samples than in the series W ones. Our data are analyzed in correlation to the deposits morphology and in terms of the occurrence of either propagation mediated reversal (collective mode linked to spatially averaged interactions at the F/AF interface) or localized switching (defect ruled mechanism taking place in a spatially confined environment). It is concluded that i) the magnetization reversal mechanism active in series W samples corresponds to a weak pinning regime propagation of walls interacting with uncompensated moments at the F/AF interface, ii) in series N samples, the magnetization reversal does not involve propagation, and iii) in the latter series the reversal events are spatially restricted to the dot-like tops of the NiO columns surrounding the membrane pores.

INTRODUCTION

Two main approaches have been considered for the coercivity enhancement in Fe-based thin films. On the one side, the coupling of the Fe-based layer to an antiferromagnetic phase[1] (this strategy entails the occurrence of exchange bias,[2] sharing with the coercivity increase an origin linked to interfacial defects). On the other,

hardening can also be achieved from the modifications of the internal dipolar fields introduced in the films by internal surfaces as those linked to antidots or other void-like morphologies.[3,4] Whereas the first approach can result in large coercivities,[5,6] it is hardly controllable (the phenomenology results from atomic scale defects originating the uncompensated moments present at the Fe/AF interface). Differently from this, the film patterning results in highly

controllable (and even predictable through simulations) coercivity increases that are moderated in magnitude since they are related to the domain walls pinning at individual motifs. Our goal in the present work is to study the reversal mechanisms associated to the combination of both hardening approaches in Fe/NiO bilayers grown onto nanostructured templates.

SAMPLES AND EXPERIMENTAL

Series N samples were grown on top of anodic alumina membranes (AAM) with a distribution of closely-packed pores having 35 nm diameters and 100 nm inter-pore distances. The membranes exhibited six-fold columnar structures surrounding each pore. The NiO layer, was deposited by magnetron sputtering, and the Fe layer grown by means of pulsed laser ablation (PLAD). We have prepared samples by implementing different oxygen partial pressures during the NiO deposition (from 0% up to 70% atomic ratio in the sputtering chamber Ar atmosphere).

The deposition of the NiO layers was carried out from a NiO target.[7] The magnetron power used was 100 W, and the atmosphere pressure was 2×10^{-2} mbar. The NiO layers had an approximate thickness of 100 nm. The Fe layers were deposited with a base pressure of 10^{-10} mbar using a laser working at 532 nm; 4 ns, 180 mJ

pulses. The Fe layers were grown with thicknesses of 5 nm, 10 nm and 20 nm (below and above the Fe correlation length, $l_{ex} = 12$ nm[8]). The bilayers were capped with a 5 nm thick Au layer deposited by evaporation.

As a reference for the comparison of series N samples behavior with that of films exclusively including interphase coupling, we also deposited, by using the same techniques and considering the same thicknesses and partial oxygen pressures, series W samples in which the Fe/NiO bilayer was deposited onto a Si wafer.

The NiO layers and Fe/NiO bilayers structure and morphology were characterized by X-rays diffraction (XRD) and atomic force (AFM) microscopy. The temperature dependence of the hysteretic properties was measured in the range from 290 K down to 50 K by means of a vibrating sample magnetometer and under fields of up to 10 kOe.

EXPERIMENTAL RESULTS

The presence of oxygen in the Ar sputtering plasma, resulted, in the series W samples, on the progressive decrease of the average NiO grain size, diminishing for 18 nm down to 4 nm when the oxygen partial pressure increased from 0% up to 70% (see a previous work of some of the authors[9]).
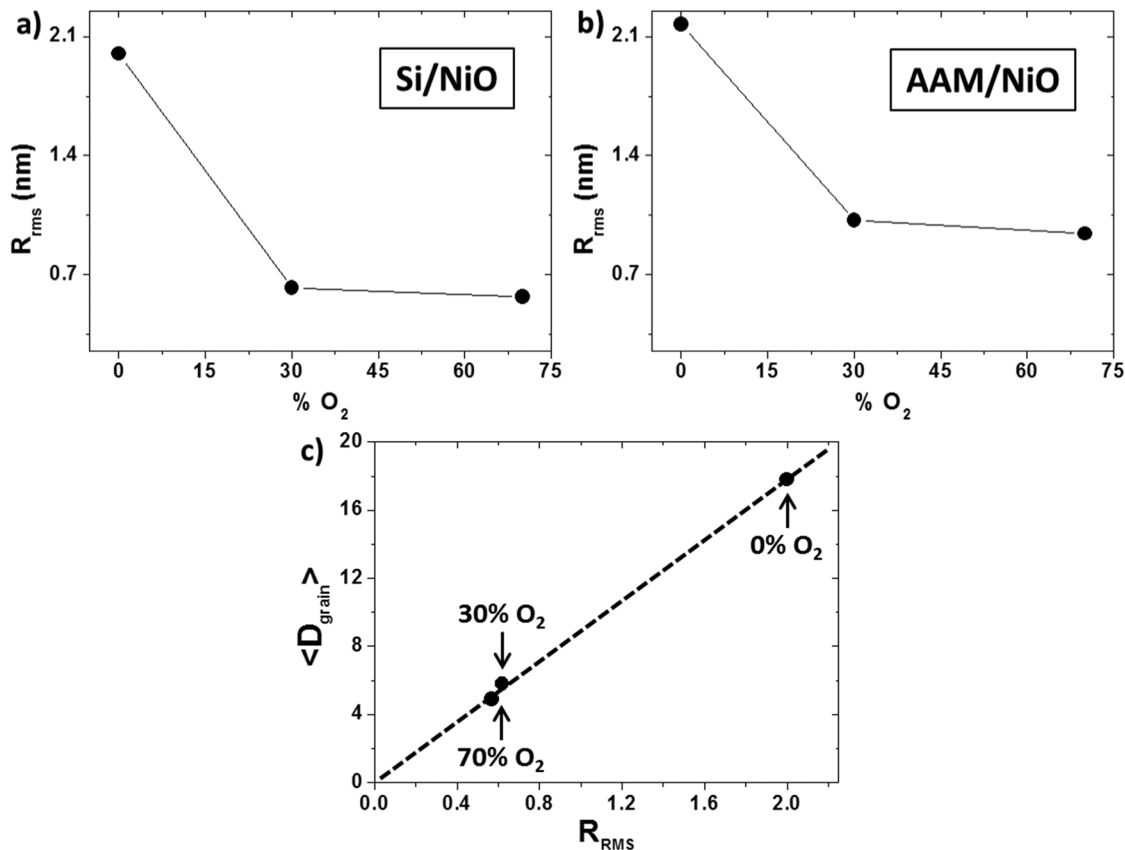

FIG. 1. a) Rms roughness in the Si/NiO layers; b) rms roughness in the AAM/NiO layers; c) proportionality between the rms roughness and the average grain size observed in the Si/NiO layers.

AFM measurements of the rms roughness, R_{rms}, of Si/NiO and AAM/NiO layers deposited using different oxygen partial pressures evidenced (see Figures 1a) and 1b), respectively) that the increase of the latter parameter resulted on a decrease of R_{rms} proportional to that observed for the average NiO grain size (as shown in Figure 1c)).

Figures 2 a), b), and c) summarize the temperature dependence of the in-plane saturation coercivity of series W samples (both series W and series N samples exhibited a parallel-to-the-substrate easy plane). From the figure is apparent that i) for a given temperature and oxygen partial pressure, the coercivity decreases with the increase of the Fe layer thickness in agreement with the size relationships between the samples thicknesses and the Fe correlation length, ii) the coercivity markedly decreases in the samples deposited under oxygen partial pressure in comparison with the pure Ar deposited samples, iii) the 50 K coercivity reaches, in the Fe 5 nm and 10 nm samples, values clearly above the anisotropy field associated the first order Fe anisotropy.

The mechanisms involved in the magnetization reversal of series W samples are collective in nature as suggested by the field evolution of the differential susceptibility evaluated at the demagnetization branch of the hysteresis loops of the samples (see Figure 3 a)): the widths at half height of the susceptibility peaks are lower than the fields corresponding to the susceptibility maxima.

Regarding the collective demagnetization of series W samples, it is interesting to point out that in these samples a propagating wall will interact with several NiO grains across its width: the NiO grains sizes range, depending on the oxygen deposition partial pressure, between 18 nm and 4 nm and the wall thickness in Fe has widths of 38 nm @ 290 K and 42 nm @ 50 K. Thus, the series W reversal process could correspond to the so-called "weak pinning regime" for which the forces hindering the wall movement are linked to the fluctuations of the number of pinning centers interacting with the wall. By assuming that the number of pinning centers at the F/AF interface is proportional to the average grain size, $<D_{grain}>$, (which can be justified considering that the pinning uncompensated moments will be preferentially accommodated at the grain boundary regions) and considering that the effective pinning force (i.e.: the coercivity) is proportional in the weak pinning regime to the fluctuations in the number of pinning centers within the wall, the coercivity, at a giving temperature, should scale with $(\delta_{Fe}/<D_{grain}>)^{1/2}$,[10] where δ_{Fe} is the Fe domain wall width at the considered temperature

Taking into account the proportionality between $<D_{grain}>$ and R_{rms} we have plotted in Figure 3 b) the coercivity variation with $(\delta_{Fe}/R_{rms})^{1/2}$. The plot, corresponding to data taken at 50 K in all the series W samples (full symbols), evidences that the saturation coercivity is, in those samples, proportional to $(\delta_{Fe}/R_{rms})^{1/2}$ and that, consequently, they switch magnetization according to a weak pinning propagation, collective mechanism. In that "weak pinning" regime the coercivity decrease associated to the increase of the NiO deposition, oxygen partial pressure should be connected to the occurrence of a more homogeneous distribution of pinning centers at the NiO/Fe interface than that present in the sample deposited with an oxygen-free sputtering atmosphere.
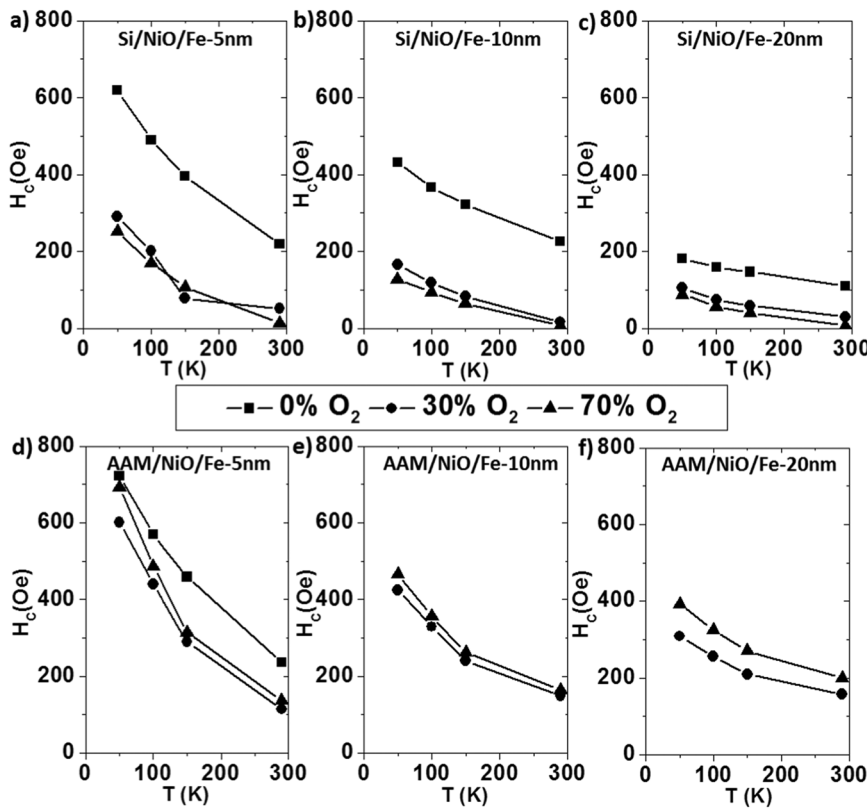

FIG. 2. Temperature dependence of the saturation coercivity of a), b) and c) series W samples and d), e) and f) series N samples.
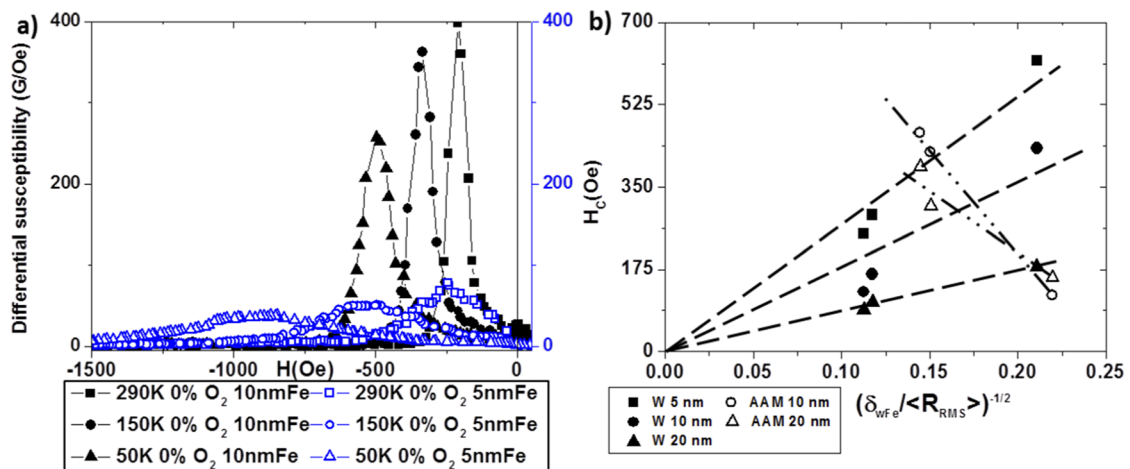
FIG. 3. a) Field dependencies of the differential susceptibilities measured at different temperatures along the demagnetizing branch of the hysteresis loop in series W, 10 nm Fe sample and series N, 5 nm sample Fe; b) dependence of the coercivity on $(\delta_{Fe}/R_{rms})^{1/2}$ (see text).

Figure 4, showing the AFM height profiles measured across-the-pores, along the lines indicated in the inset, confirms that the pores are still open after the bilayer deposition is completed for the thickest Fe layer. Also, AFM height profiles measured across two neighbouring columns in the series N, Fe 20 nm bilayer sample show that the tops of the columns around a pore are separated by trenches having, at least, 5 nm depth.

The hysteretic behavior of the series N samples is shown in Figure 2 d), e) and f), where we have represented the variation with the temperature of the in-plane saturation coercive force measured in samples with different Fe layer thicknesses and with NiO layers grown by using different oxygen partial pressures.
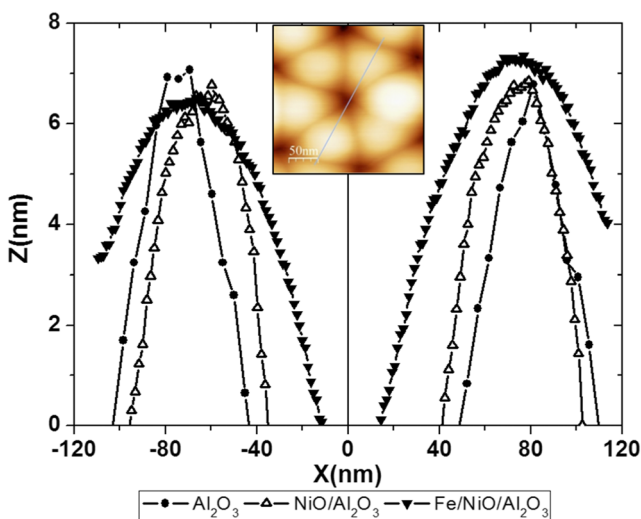
As in the case of series W samples, the coercivity decreases at all the temperatures with the increase of the Fe layer thickness. Despite that similar behavior, series N samples show a lower decrease of the coercive force with the increase of the oxygen partial pressure than that observed in the samples in the former series. It is also worth to point out that the coercivity found on the series N, 5 nm Fe sample is the larger we have measured and giant in the sense that it is above the anisotropy field corresponding to first order Fe anisotropy constant.

We have plotted in Figure 3 b) (open symbols) the dependence of the series N saturation coercivity with the $(\delta_{Fe}/R_{rms})^{1/2}$ quantity. Our results evidence that series N samples do not demagnetize according to collective, weak pinning mechanisms (our data do not extrapolate to zero coercivity for zero fluctuation of the number of defects inside the wall). This point is endorsed by the field dependence of the differential susceptibility measured along the demagnetization branch of the loop in series N samples (Figure 3 a)), from which it is apparent that the field distribution of partial demagnetizations is in series N much broader than in series W. In series N, the coercivity decrease linked to the presence of oxygen in the NiO atmosphere deposition could be related to the local decrease of the effective anisotropy acting over the interfacial uncompensated moments originated by the presence of interstitial oxygen (resulting on magnetic bonds breaking).

The non-collective, local character of the demagnetization of the series N samples can be traced to the AFM observed morphology of the corresponding Fe layers, that, as shown in Figure 4 is associated to a six-fold structure surrounding the AAM, non-obturated pores and mutually separated by trenches at least 5 nm deep. According to this morphology, and considering that the inter-lobes trenches can effectively act as strong pinning centres for the propagation of the magnetization reversal from a switched lobe to its neighbours, the global sample reversal could proceed independently at different regions of the sample. Consequently, the reversal process in series N samples should be mostly ruled by the local defects (uncompensated moments at the F/AF interface) distribution.

FIG. 4. AFM profiles taken along lines crossing the samples pores (see the image inset) corresponding to the alumina membrane, the AAM/NiO layer and the AAM/NiO/Fe 20 nm bilayer.

CONCLUSIONS

We have shown that in the case of the Si/NiO/Fe samples the coercivity mechanism is a collective one, linked to the interaction (weak pinning) of propagating walls with several defects/ unbalanced interfacial moments across the wall width. Optimization of the coercivity in these samples should involve growth of larger grains/roughness wave lengths in the NiO layers (avoiding oxygen partial pressures in the sputtering atmosphere). Differently from this, in the AAM/NiO/Fe samples the magnetization reversal is mostly local and bounded to the tips of the columnar structures surrounding the membrane pores. In these samples the deteriorating influence of the oxygen partial pressures is smaller than in the Si/NiO/Fe samples.

ACKNOWLEDGMENTS

REFERENCES

[1] O. Zaharko, P. M. Oppeneer, H. Grimmer, M. Horisberger, H. Ch. Mertins, D. Abramsohn, F. Schäfers, A. Bill, and H.-B. Braun, Phys. Rev. B **66**, 134406 (2002).

[2] J. Nogués and I. K. Schuller, J. Magn. Magn. Mater. **192**, 203 (1999).

[3] F. Pigazo, F. García Sánchez, F. J. Palomares, J. M. González, O. Chubykalo-Fesenko, F. Cebollada, J. M. Torres, J. Bartolomé, and L. M. García Vinuesa, J. Appl. Phys. **99**, 08S503 (2006).

[4] E. Paz Pérez de Colosía, F. Cebollada Baratas, F. J. Palomares Simón, J. M. González, Mi-Y. Im, and P. Fischer, J. Appl. Phys. **111**(7), 073908 (2012).

[5] M. Mansuripur, J. Appl. Phys. **61**, 1580 (1987).

[6] C. Prados, P. Crespo, J. M. González, A. Hernando, J. F. Marco, R. Gancedo, N. Grobert, M. Terrones, R. M. Walton, and H. W. Kroto, Phys. Rev. B **65**(11), 113405-1–113405-4 (2002).

[7] A. Gutiérrez, G. Domínguez-Cañizares, J. A. Jiménez, I. Preda, D. Díaz-Fernández, F. Jiménez-Villacorta, G. R. Castro, J. Chaboy, and L. Soriano, Appl. Surface Sci. **276**, 832 (2013).

[8] G. S. Abo, Y.-K. Hong, J. Park, J. Lee, W. Lee, and B.-C. Choi, IEEE Trans. on MAGNETICS **49**(8), 4937 (2013).

[9] G. Domínguez-Cañizares, A. Gutiérrez, J. Chaboy, D. Díaz-Fernández, G. R. Castro, and L. Soriano, Journal of Materials Science **49**(7), 2773–2780 (2013).

[10] R. Skomski and J. M. D. Coey, *Permanent Magnetism* (CRC Press, 1999).